Korean J. Chem. Eng., 37(5), 839-849 (2020)
DOI: 10.1007/s11814-020-0500-y

pISSN: 0256-1115
eISSN: 1975-7220

Particle resolved CFD simulation on vapor-phase synthesis of vinyl acetate from ethylene in fixed-bed reactor

Yonghui Li*,, Mingkai Wang*,**, Xingxing Cao*,**, and Zhongfeng Geng*,**,†**

*Key Laboratory for Green Chemical Technology of Ministry of Education,
R&D Center for Petrochemical Technology, Tianjin University, Tianjin 300072, China
**Collaborative Innovation Center of Chemical Science and Engineering, Tianjin 300072, China
(*Received 4 September 2019 • accepted 31 January 2020*)

Abstract−The synthesis of vinyl acetate (VAc) from ethylene is a strongly exothermic reaction that might easily cause catalyst deactivation and reduce selectivity of VAc. Research at the bed scale helps to improve the conversion of C_2H_4 and the selectivity of VAc. In this study, the discrete element method (DEM) was used to construct a fixed-bed structure model via simulating the filling process of catalyst particles in the reactor. The inlet section of a reaction tube was studied, and its length was 10 cm. The temperature distribution, and the effects of particles size, inlet velocity, inlet temperature and the feed ratio of C_2H_4 to O_2 on the reaction process were studied. Simulated results show that the bed temperature gradually increased from the wall to the center, and the temperature gradient gradually decreased along the radial direction. The maximum temperature was 438.68 K and the temperature difference from the inlet temperature was 5.54 K. Comparing the composite particle packed bed with the single particle size packed bed, the composite packed bed has higher vinyl acetate selectivity. Increasing inlet velocity from 1.5 m/s to 3.5 m/s, the selectivity of vinyl acetate increased from 91.71% to 92.60%. Adding an inert gas to the feed gas can increase the oxygen concentration and reduce the explosion interval of C_2H_4, the conversion of C_2H_4 and the selectivity of vinyl acetate increased.

Keywords: DEM, CFD, Fixed Bed Reactor, Synthesis Of Vinyl Acetate, Selectivity

INTRODUCTION

Vinyl acetate (VAc), an unsaturated carboxylic acid ester, is an important organic chemical raw material used in the production of polyvinyl acetate (PVAc), polyvinyl alcohol (PVA), vinyl acetate-vinyl copolymer emulsion (VAE), copolymer resin (EVA), vinyl chloride-vinyl acetate copolymer (EVC), polyacrylonitrile copolymer and acetal resin. These products are widely used in the chemical industry, light industry, machinery, agriculture and other fields [1-4]. In recent years, the production capacity of VAc has shown steady growth. According to current projections, the worldwide production capacity of VAc will reach 9 million tons by 2020.

At present, the production route of VAc is mainly divided into two types: vapor phase synthesis of vinyl acetate from acetylene method and vapor phase synthesis of vinyl acetate from ethylene method. The vapor-phase synthesis of vinyl acetate from ethylene has the advantages of high product quality, fewer environmental hazards and high energy efficiency. Consequently, it occupies a dominant position in the VAc industry [5-8]. In the fixed-bed reactor, the exothermic reaction of ethylene synthesis of vinyl acetate faces three major problems: (1) The temperature distribution of the catalyst bed is not uniform, so that the catalyst in the high temperature region is first deactivated; (2) Improper design or operation can cause a decrease in the selectivity of the catalyst in the reactor; (3) To prevent intense combustion and explosive limit of ethylene in the reactor, the O_2 content of the feed gas is limited, which in turn affects the single pass conversion of C_2H_4 [9]; the chemical reaction equation for the main reaction is [10]:

$$CH_3COOH+C_2H_4+0.5O_2=CH_3COOC_2H_3+H_2O,\ \Delta H=-176.53\ kJ/mol,$$

and the side reaction is:

$$C_2H_4+3O_2=2CO_2+2H_2O,\ \Delta H=-1{,}339.8\ kJ/mol.$$

The key step in the production process is to improve the selectivity of the catalyst and ensure the timely removal of the reaction heat. In the reaction of synthesis of vinyl acetate from ethylene, the molar ratio of C_2H_4 to O_2 is 2 : 1. However, C_2H_4 is always excessive, which is mainly affected by the explosion interval of C_2H_4 in actual production. According to the index of oxygen partial pressure in the reaction kinetic equation established by researchers [11,12], it can be concluded that the main reaction is more sensitive to the change of oxygen concentration than the side reaction, the activation energy of the side reaction is higher than that of the main reaction, and the side reaction is more sensitive to temperature changes [13].

Packed beds of particles are widely used in chemical reactors, separators, filters, dryers and heat exchangers [14,15]. Research and optimization of its internal flow and heat transfer are of great significance to improve energy efficiency. When the tube-to-particle diameter ratio (D/dp) is small, the pressure drop in the bed is reduced and the heat transfer efficiency is improved. These advantages have

†To whom correspondence should be addressed.
E-mail: zfgeng@tju.edu.cn

attracted more and more attention. The small tube-to-particle diameter ratio (2≤D/dp<10) is the latest development trend of a traditional particle packed bed [16]. Logtenberg and Dixon [17] used CFD to simulate a fixed bed of tube to particle ratio 2.86 and obtained the temperature field and the heat transfer coefficient between the fluid and tube wall in the bed. Jiang et al. [18] predicted the particle-to-fluid heat transfer coefficients and provided details of the fluid flow inside the miniporous media using lumped capacitance method and CFD method. Guardo et al. [19] used CFD simulation to investigate the effect of turbulence model on fluid-wall heat transfer coefficient. Gunjal et al. [20] studied fluid flow through the array of spheres using the unit-cell approach, in which different periodically repeating arrangements of particles such as simple cubical, 1-D rhombohedral, 3-D rhombohedral, and face-centered cubical geometries were considered.

The synthesis of vinyl acetate from ethylene generally occurs in a tubular fixed-bed reactor [21-23]. These reactors have the advantages of large heat transfer area, high heat transfer efficiency and good operation performance. Therefore, they are widely used in strong exothermic and strong endothermic chemical reaction processes [24,25], such as oxidation of n-butane to maleic anhydride [26], phthalic anhydride from o-xylene [27], the synthesis ethylene oxide [28], and methane steam reforming [29,30]. The accumulation of catalyst particles in a fixed-bed reactor is complicated, and the construction of the bed structure is the basis for accurately simulating the properties of the flow field and temperature field. Vollmari et al. [31] calculated pressure drops in packings of spherical and non-spherical particles of varying sizes by DEM-CFD approach. Simulated results from the DEM-CFD are benchmarked against the experiments, the results are in very good agreement for spheres. Zhou et al. [32] used CFD to simulate a coupled acetone hydrogenation reaction in a fixed bed. The results show that the smaller particle size is beneficial to accelerate the reaction rate, but it will increase the bed pressure drop. Mandar et al. [33] used CFD-DEM method to simulate the packed bed. Two segments, a cut segment and a wall-segment, have been proposed to represent the core central region of packed bed and near wall region of packed bed, respectively, which offer a computationally efficient way of understanding the transport phenomena in an industrial scale reactor. Gregor et al. [29] simulated dry reforming of methane over nickel in a fixed-bed reactor of spheres which was studied with CFD simulation, and the result predicted the area where the catalyst surface is first deactivated in the fixed bed.

In this paper, the simulation tool used was STARCCM+12.02 commercial software developed by CD-adapco. The process of spherical catalyst particles filling in the reaction tube was first simulated by the DEM method. A three-dimensional fixed bed reactor model was employed. The inlet section of reaction tube with a length of 10 cm was studied. The CFD physical model of the flow, heat transfer and reaction process in the bed was established by adding the reaction kinetics model on the catalyst. The distribution of the temperature field and the concentration field in the bed was obtained. The causes of the local high temperature position were studied, and the effects of particle size, inlet velocity, inlet temperature and feed ratio of the raw material on the reactor temperature and selectivity of VAc were investigated.

PHYSICAL AND MATHEMATIC MODEL

1. Geometric Model

A fixed-bed reactor is composed of thousands of reaction tubes, so it is feasible to select one reaction tube for simulation due to the

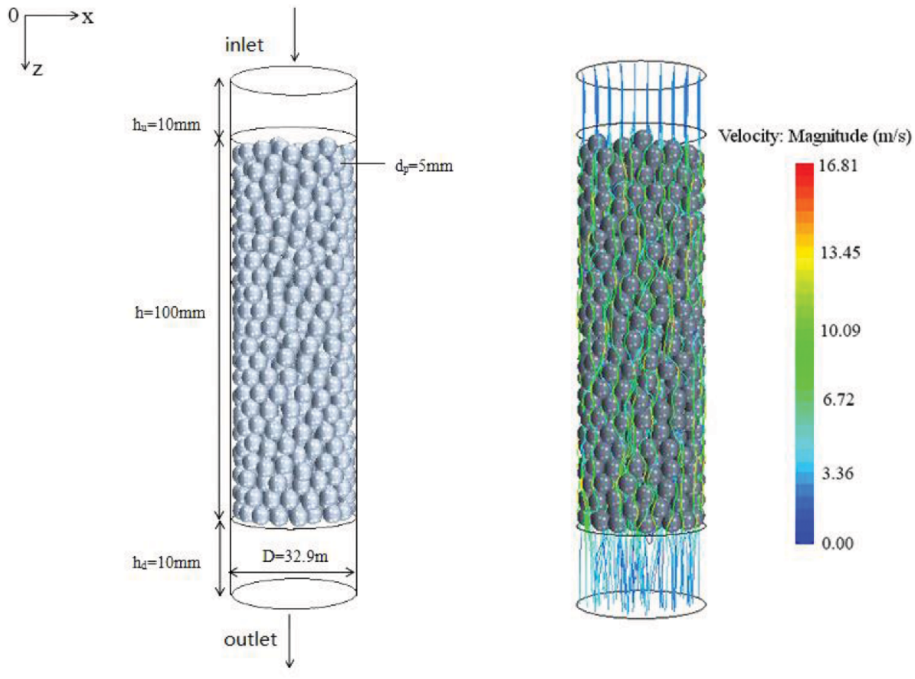

(a) The geometric structure of catalyst bed (b) The fluid domain

Fig. 1. The geometric structure of catalyst bed in reaction tube and the fluid domain.

Table 1. Parameters in the DEM model

Material properties	Parameter
Density of catalyst particles (kg/m^3)	1500
Poisson's ratio of catalyst	0.17
Young's modulus of catalyst (GPa)	73.105
Coefficient of friction	0.4
Rolling drag coefficient	0.001

similar internal conditions of different reaction tubes. In this study, the bed structure was constructed by DEM. To avoid the boundary effect, it was increased by 10 mm in the upper stage and the lower stage of the tube, respectively. The catalyst bed and fluid domain are as shown in Fig. 1(a) and Fig. 1(b). Fig. 1(a) is the geometric structure of catalyst bed, and Fig. 1(b) is the fluid domain. As shown in Fig. 1(a), the inlet section of a reaction tube is studied and the bed height is 100 mm, The total length of the reaction tube model is 120 mm. The inner diameter of the tube is D=32.9 mm, the particle diameter is dp=5 mm, and the tube-to-particle diameter ratio is N=6.58. The parameters of the reaction tube and catalyst in the DEM model are shown in Table 1. The mass flow rate of the particles was set to 0.01 kg/s. When the height of particle accumulation is 100 mm and the velocity of all particles is lower than 10^{-7} m/s, when the particles no longer fall, the bed structure is in a stable state. The number of particles is 749, the average void ratio $\overline{P}$ is 0.427, and the error associated with the empirical correlation (1) proposed by Dixon [34] is 2.37%.

$$\overline{P}=0.4+0.05(d_p/d_t)+0.412(d_p/d_t)^2 \quad d_p/d_t\le 0.5 \tag{1}$$

Table 2. Physical properties of the inlet gas mixture and boundary conditions

Physical property	Vslue
Inlet molar ratio C_2H_4 : CH_3COOH : O_2	12 : 4 : 1
Density (kg/m^3)	1.45
Thermal conductivity of gas (W/m·K)	0.065
Specific heat (J·kg^{-1}·K^{-1})	2104
Dynamic viscosity (m^2·s^{-1})	1.06E-5
Molecular diffusivity (m^2·s^{-1})	2.53E-6
Inlet velocity (m·s^{-1})	2.5
Inlet temperature (K)	433.15
Wall temperature (K)	433.15
Operating pressure (MPa)	0.8

2. Physical Model

The boundary conditions of the inlet section of the reaction tube are set as: velocity inlet, pressure outlet, and the wall surface is constant temperature. The physical properties of the inlet gas and operating parameters are shown in Table 2. In this paper, it is assumed that the physical properties of the gas phase are not a function of temperature.

3. Grid Independence Test and Model Validation

To ensure that the simulation results were independent of the grid system, the grid independence was checked. Unstructured polyhedral meshes were made in the fluid domain and the grid size was set to 2 mm, 1 mm, 0.5 mm, 0.4 mm, respectively. The number of cells was 1.08 million, 3.12 million, 5.58 million 6.21 million, respectively. The number of prism layers was set to 2. To improve the mesh

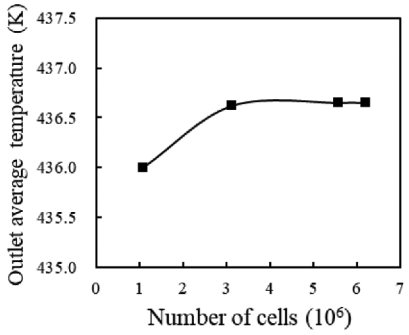

(a) Effect on outlet average temperature of cells

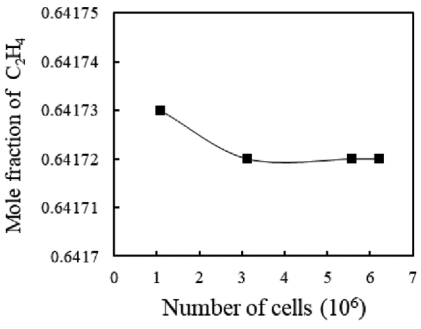

(b) Effect on mole fraction of C_2H_4 of cells

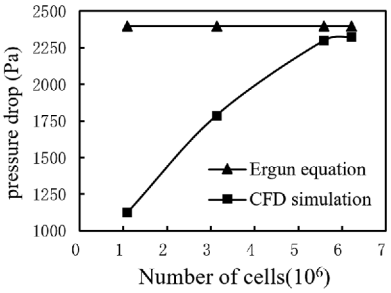

(c) Effect on the pressure drop of cells

Fig. 2. Effect of number of cells.

quality of contact-points between particles, the particles were locally flattened [35,36]. As shown in Fig. 2(a), the average temperature at the outlet first increases correspondingly with the number of cells, and finally stabilizes at 436.7 K. It is also clear in Fig. 2(b) that the mole fraction of ethylene decreases first as the number of cells increases, and finally stabilizes at 0.641 72. The above results indicate that when the basic size of the cell is 0.5 mm, with the increase of the number of cells, the results no longer change. Considering the simulation accuracy and computer time consumption, the grid division method with the basic size of 0.5 mm was selected. The CFD model in this work was validated by comparing the predicted results of pressure drop against Ergun equation. Fig. 2(c) shows that the numerical results agreed well with the empirical correlations, the numerical results deviate by less than 5% from the Ergun equation, which allowed us to apply the numerical method to the studies in the present work.

4. Governing Equations

For the simulations in this study, full three-dimensional governing equations were applied. In the calculation domain, the velocity, pressure, temperature, and component concentration of the gas are solved by the control equations. The ethylene synthesis of vinyl acetate in the fixed bed reactor can be described by the following control equations [37]:

Conservation of mass:

$$\nabla\cdot(\rho \mathrm{v})=0 \tag{2}$$

Mass conservation equation of gas phase component:

$$\nabla\cdot(\rho c_g \mathrm{v} w_i)=\nabla\cdot(\rho D_i \nabla w_i)+v_i M_i F\sum_{j=1}^{N_R} r_j \tag{3}$$

where the first term on the right of the equals sign represents the mass diffusion, and the second term represents the reaction source term.

Conservation of momentum:

$$\nabla\cdot(\rho \mathrm{v}\times \mathrm{v})=-\nabla P+\nabla\cdot(\mu(\nabla \mathrm{v}+(\nabla \mathrm{v})^{\mathrm{T}})) \tag{4}$$

Energy conservation equation:

$$\nabla\cdot(\rho c_g \mathrm{v} T_g)=\nabla\cdot(h_g \nabla T_g)+F\sum_{j=1}^{N_R}((-\Delta H_j) r_j) \tag{5}$$

5. Reaction Kinetics Model

In this paper, we chose a method of adding one-step main reaction and one-step side reaction to couple the reaction source term, which was proposed by Zhao et al. [38] and it can be written as:

$CH_3COOH+C_2H_4+0.5O_2=CH_3COOC_2H_3+H_2O$

Reaction rate of main reaction:

$$r_1=1.5464\exp\left(\frac{-71.94}{RT}\right)P_{O_2}\ \mathrm{mol/(g\cdot min)} \tag{6}$$

$C_2H_4+3O_2=2CO_2+2H_2O$

Reaction rate of side reaction:

$$r_2=1.0972\times10^6\exp\left(\frac{-109.37}{RT}\right)P_{O_2}^{0.5}\ \mathrm{mol/(g\cdot min)} \tag{7}$$

In the main reaction, the index of oxygen partial pressure is 1. In the side reactions, the index of oxygen partial pressure is 0.5. In this paper, the chemical reaction is modeled to occur only to the surface of the catalyst particles.

6. Turbulence Model

$$\mathrm{Re}_p=\frac{\rho v_{in} d_p}{\upsilon} \tag{8}$$

When $\mathrm{Re}_p>300$, the flow is highly unstable and chaotic, close to turbulent. Therefore, this flow regime can be approximated by Reynolds-Average Navier-Stoke (RANS) turbulence: $v_i=\overline{v_i}+v_i'$.

The turbulence equation is as follows:

$$\frac{\partial}{\partial t}(\rho\kappa)+\frac{\partial}{\partial x_j}(\rho\kappa u_j)=\frac{\partial}{\partial x_j}\left[\left(\mu+\frac{\mu_t}{\sigma_k}\right)\frac{\partial \kappa}{\partial x_j}\right]+G_\kappa+G_b-\rho\varepsilon-Y_M+S_\kappa \tag{9}$$

$$\frac{\partial}{\partial t}(\rho\varepsilon)+\frac{\partial}{\partial x_j}(\rho\kappa u_j)=\frac{\partial}{\partial x_j}\left[\left(\mu+\frac{\mu_t}{\sigma_k}\right)\frac{\partial \varepsilon}{\partial x_j}\right]+\rho C_1 S\varepsilon-\rho C_2\frac{\varepsilon^2}{\kappa+\sqrt{\upsilon\varepsilon}}+C_{1\varepsilon}\frac{\varepsilon}{\kappa}C_{3\varepsilon}G_b+S_\varepsilon \tag{10}$$

$$C_1=\max\left[0.43,\ \frac{\eta}{\eta+5}\right] \tag{11}$$

$$\eta=S\frac{\kappa}{\varepsilon} \tag{12}$$

$$\mu^*=\sqrt{S_{ij}S_{ji}+\Omega_{ij}\Omega_{ji}} \tag{13}$$

$$\Omega_{ij}=\Omega_{ij}-2\varepsilon_{ijk}\omega_\kappa \tag{14}$$

$$\Omega_{ij}=\overline{\Omega_{ij}}-\varepsilon_{ijk}\omega_\kappa \tag{15}$$

$$A_0=4.04,\ A_S=\sqrt{6}\cos\varphi \tag{16}$$

$$\varphi=\frac{1}{3}\cos^{-1}(\sqrt{6}W),\ W=\frac{S_{ij}S_{jk}S_{ki}}{S^3},\ S=\sqrt{S_{ij}S_{ji}},\ S_{ij}=\frac{1}{2}\left(\frac{\partial \mu_j}{\partial x_i}+\frac{\partial \mu_i}{\partial x_j}\right) \tag{17}$$

RESULTS AND DISCUSSION

1. Temperature Distribution

The synthesis of vinyl acetate from ethylene is an exothermic reaction. To prevent the local temperature from being too high, it is necessary to remove reaction heat in the production process. Therefore, the investigation of the temperature distribution in the reaction tube helps to understand the formation of high temperature and low temperature regions. In this study, the inlet temperature and wall temperature were set to 433.15 K. Fig. 3(a) shows the axial temperature contours of fluid. The maximum temperature is 438.68 K and the temperature difference from the inlet temperature is 5.54 K. Fig. 3(b) shows the radial temperature contours of fluid. In the same cross section, the temperature near the contact points of the particles is higher, and the maximum temperature difference from the wall temperature is about 5 K.

As shown in Fig. 4(a), the radial average temperature of the fluid gradually increases from the wall to the center of the tube. The temperature gradient is the largest near the wall and smallest near the center of the tube. The radial maximum average temperature difference is 0.98 K. Fig. 4(b) shows the axial average temperature distribution of the fluid. It can be seen that the average temperature gradually increases along the axial direction, and the highest tem-

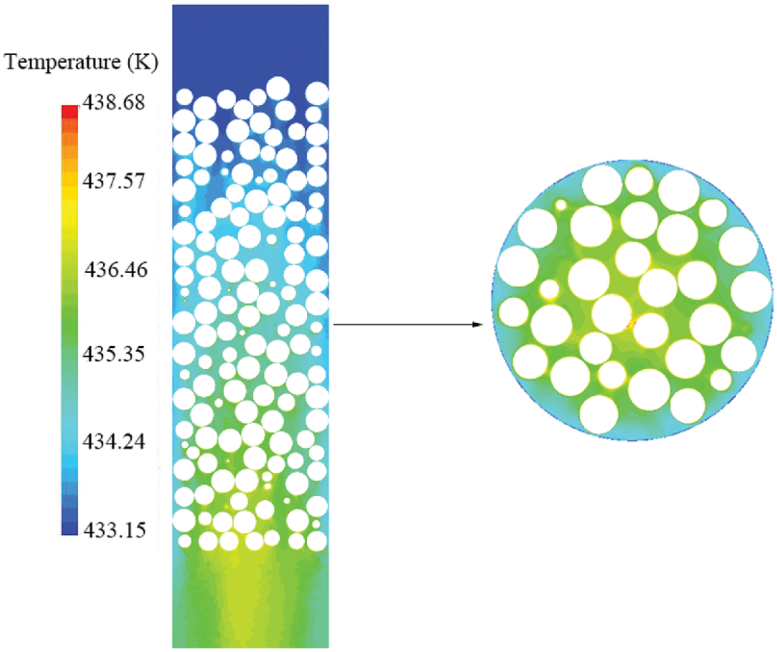

（a）Section in the axial direction （b）Section in the radial direction

Fig. 3. The temperature distribution of the fluid in the cross section.

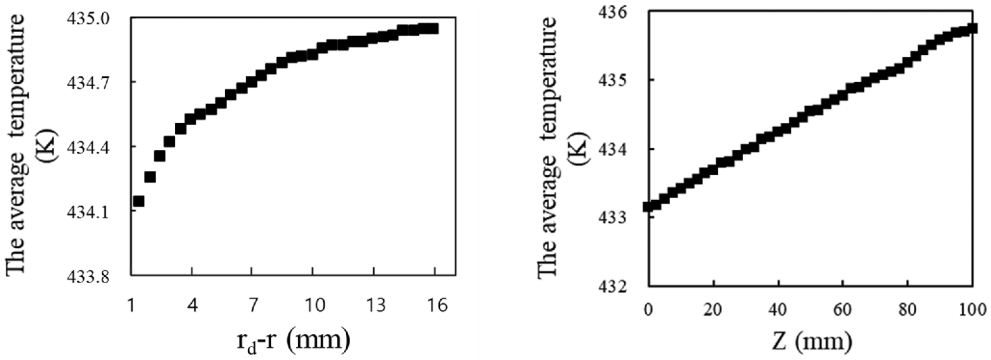

(a) The radial average temperature (b) The axial average temperature

Fig. 4. The average temperature distribution of the fluid.

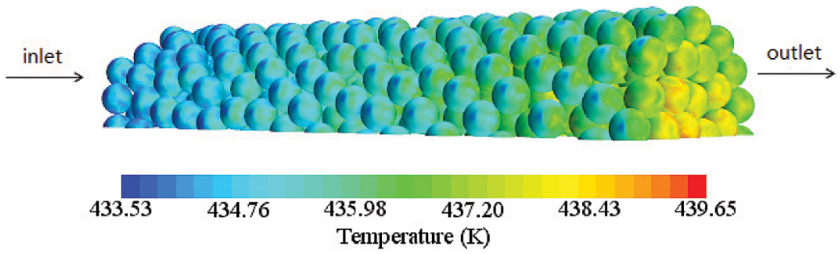

Fig. 5. The temperature distribution at the surface of the catalyst particles.

perature is at the outlet of the reaction tube. Fig. 5 shows the temperature profile at the surface of the catalyst particles, it can be seen that the temperature of the surface of the catalyst particles also increases along the radial and axial directions, and the temperature of the particles at the bottom of the bed is the highest. At different positions on the surface of the same catalyst particle, the flow rate and the reaction rate are different, resulting in uneven temperature distribution on the surface of the particle. Stagnation occurs when the gas flows through the bottom of the particle, so the temperature at the bottom of the particle is the highest; therefore, the

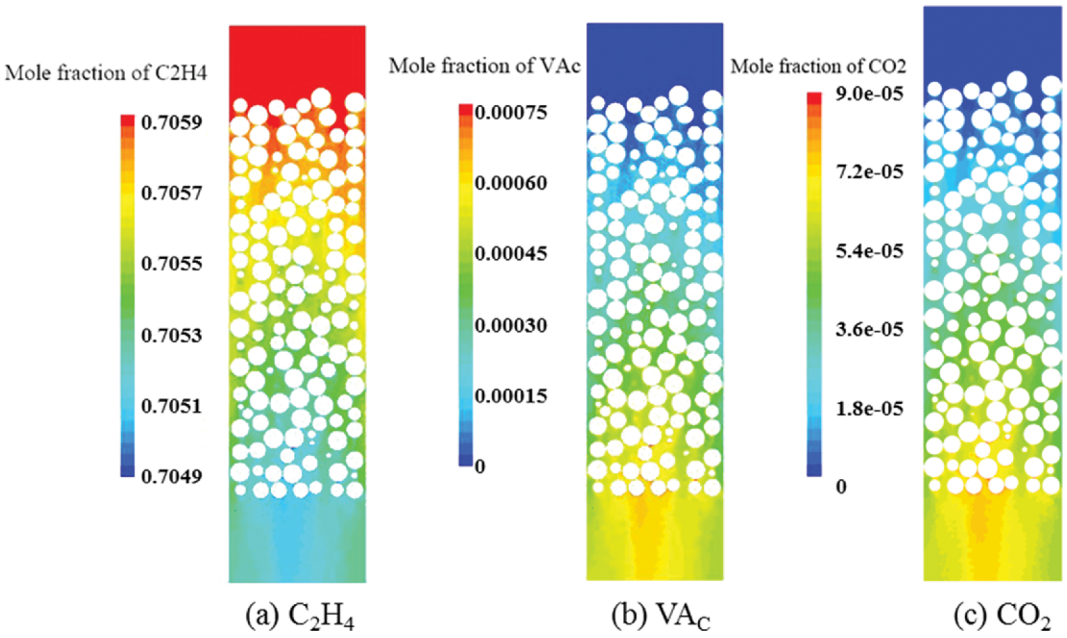

Fig. 6. The distribution of mole fraction of C_2H_4, VAc, and CO_2 in the fixed bed.

catalyst at this position is easily deactivated.

2. Concentration Distribution

Fig. 6 shows the mole fraction distribution of the reactant C_2H_4, the target product VAc, and the by-product CO_2. As shown in Fig. 6(a), the molar fraction of C_2H_4 gradually decreases along the axial and radial direction. Comparing Fig. 6(b) with Fig. 6(c), the concentration of the target product VAc and by-product CO_2 gradually increases in both the radial direction and the axial direction. The molar fraction of CO_2 is 0.16-times that of the target product VAc at the outlet of the tube.

3. Reaction Rate Distribution

In the kinetic model, two key factors limit the reaction rate: the temperature of the gas and the partial pressure of oxygen. As the reaction progresses, the released heat causes an increase in temperature, which accelerates the reaction rate. On the other hand, the oxygen concentration decreases, resulting in a decrease in the reaction rate. Therefore, the reaction rate is affected by the combination of temperature and partial pressure of oxygen.

The distribution of the reaction rate at the surface of the catalyst particles is shown in Fig. 7. The inlet temperature and wall temperature were set to 433.15 K. Because of the symmetry of the structure of the bed, a half-volume bed is selected to show. The simulation results are close to the results of Zhao [36], who studied the synthesis of vinyl acetate from ethylene-gas by single-reaction tube experimental research. It can be seen that the reaction rate gradually increases along the axial and radial direction. The reaction rate at the center of the outlet is the highest. The reaction rate is also different on the surface of the same catalyst particle. Comparing Fig. 5 with Fig. 7, it can be found that the reaction rate distribution is similar to temperature distribution. Therefore the reaction rate is greatly affected by temperature.

4. Effects of Single Particle Size

All other parameters remain unchanged, the diameter of catalyst was set to 3 mm, 4 mm, 5 mm, 6 mm, respectively. It can be concluded from Fig. 8(a) that the radial average temperature gradually increases from the wall to the center of the tube. As the particle diameter increases, the radial average temperature gradually decreases. Fig. 8(b) shows the effect of particle diameter on the axial temperature distribution. As the particle diameter increases, the axial average temperature is also gradually increased. Therefore, properly increasing the particle diameter contributes to the transfer of heat and prolongs the catalyst lifetime. Because the larger catalyst

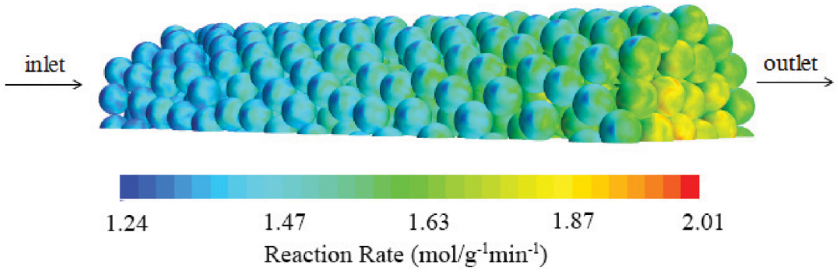

Fig. 7. Distribution of the main reaction rate at the surface of catalyst particles.

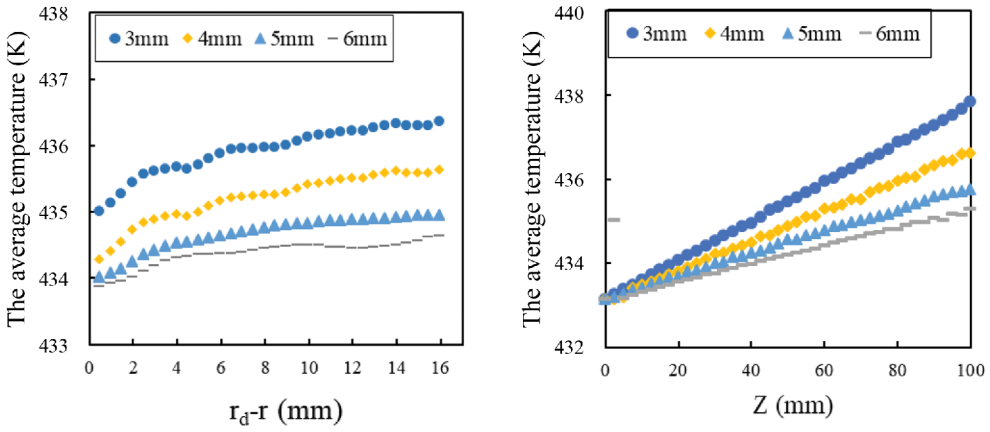

(a) The radial average temperature (b) The axial average temperature

Fig. 8. The average temperature distribution at different single particle sizes.

Table 3. Molar fraction and VAc selectivity on the outlet of the fixed-bed at different particle diameters

Particle diameter (mm)	C_2H_4 (10^{-1})	VAc (10^{-4})	CO_2 (10^{-4})	Selectivity (%)
3	7.0445	8.7562	1.8768	90.32
4	7.0476	6.8830	1.2182	91.87
5	7.0499	5.2324	0.8674	92.35
6	7.0512	4.2507	0.3486	92.42

pellets have a higher void fraction, this presents less area for reaction and generates less heat. High porosity also helps heat transfer and reduces bed temperature.

Table 3 compares the mole fraction of each component at the outlet and the selectivity of vinyl acetate at different particle sizes. It can be seen that as the particle diameter increases, the molar fraction of ethylene at the outlet increases, the molar fraction of vinyl acetate decreases, and the selectivity of vinyl acetate increases from 90.32% to 92.42%. The result indicates that increasing the particle diameter helps to reduce the temperature rise of the fluid, thereby increasing the conversion of ethylene and the selectivity of vinyl acetate.

5. Effects of Composite Particle Size

To compare the equally proportioned packed bed of 5 mm and 6 mm particles with 5.5 mm single particle size packed bed, Table 4 shows the mole fractions of each component at the outlet and the selectivity of vinyl acetate at the outlet. It can be concluded that the composite packed bed has lower conversion of C_2H_4, lower bed temperature and higher vinyl acetate selectivity than single diameter packed bed.

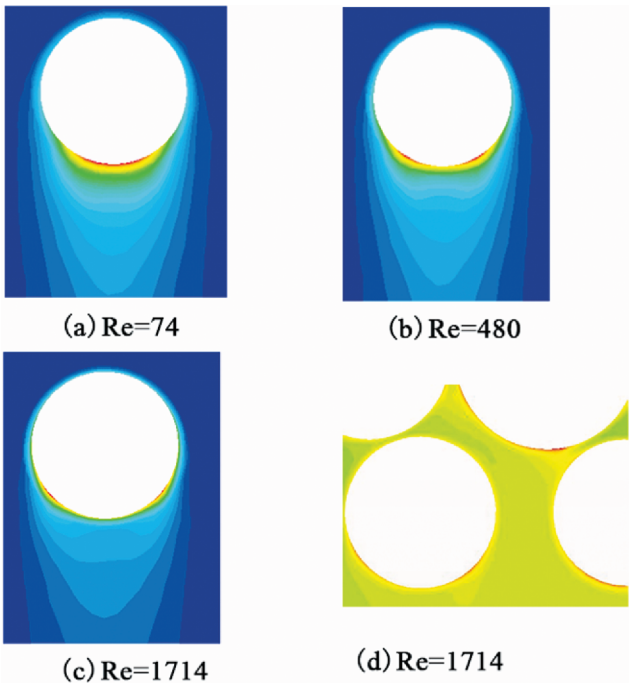

Fig. 9. Influence of Reynolds number and particles on temperature distribution.

6. Effects of Inlet Velocity

Inlet velocity has an important influence on fluid flow and heat transfer. To study effects of inlet velocity on temperature distribution, first, the temperature distribution on the surface of a single catalyst particle was investigated. As can be seen from Fig. 9, at lower

Table 4. Molar fraction and VAc selectivity at the outlet with different bed structure

Particle diameter (mm)	C_2H_4 (10^{-1})	VAc (10^{-4})	CO_2 (10^{-4})	Selectivity (%)	Highest temperature (K)
5.5	7.0502	4.9946	0.8240	92.38	438.25
5+6	7.0506	4.7424	0.7801	92.40	438.13

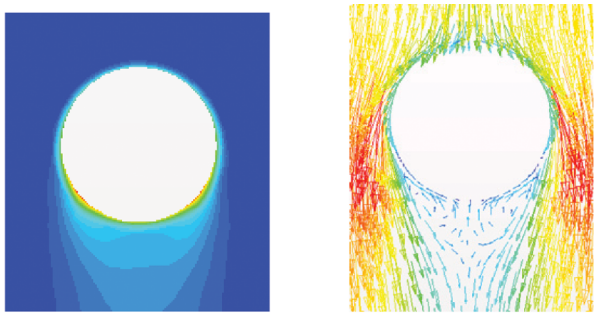

(a) velocity contour (b) velocity vector fields

Fig. 10. The distribution of flow field around a single particle at Re= 1714.

Re, the highest temperature is directly below the particle. When the Re is increased from 72 to 1714, the highest temperature gradually moves to the position on both sides of the bottom of the particle, indicating that inlet velocity affects not only the magnitude of temperature but also the temperature distribution. The reason for this phenomenon is that when the Re=74, the inlet velocity≈0.1 m/s, and the flow type is laminar flow. The fluid flows along the surface of the particles, then converges at the bottom of the particles and forms a high temperature zone at the bottom of the catalyst particles. When the Re=1714, the inlet velocity is 2.5 m/s, the flow type is turbulent flow. As shown in Fig. 10, when the flow velocity is high, after the fluid bypasses the top of the catalyst particles, it flows to both sides of the particles and forms a high-speed area. A significant low-speed area appears directly below the bottom of the particles, and it is easy to cause retention or back flow. So the highest temperature appears on sides of the bottom of the particle. Fig. 9(d) shows the temperature field of the cross-section of the bed. Since the bed is composed of many particles, the temperature distribution around a particle is affected by the surrounding pore structure. Comparing Fig. 9(b) with Fig. 9(d), one can find that the temperature distribution of the surface of the particles in the bed is similar to that of a single particle, but there is no strict symmetry.

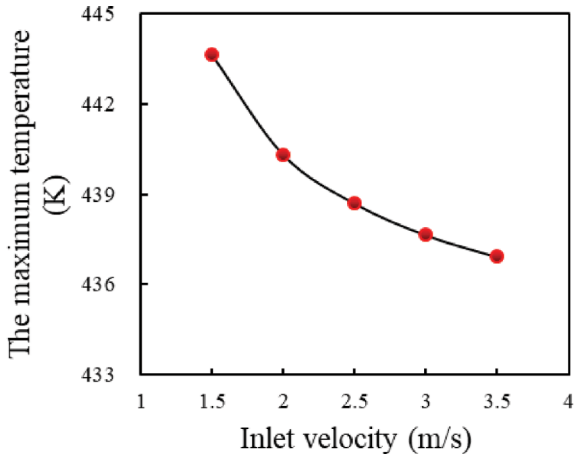

Fig. 12. The maximum temperature in the bed at different inlet velocity.

All other parameters remain unchanged, the inlet velocity of the raw gas is increased from 1.5 m/s to 3.5 m/s with a step size of 0.5 m/s. The fluid domain of the inlet velocity of 2.5 m/s is shown in Fig. 1(b). The fluid first maintains a stable axial flow through the upper extension of the bed, and then flows into the catalyst bed. According to the streamline, the flow direction is tortuous and the velocity distribution is uneven. The highest velocity of the gas phase is 16.81 m/s, which is 6.72-times the inlet velocity of 2.5 m/s. After that, the fluid flows out the bed. Fig. 11 shows the radial and axial distribution of the mean temperature, respectively. Increasing the inlet velocity helps to reduce the mean bed temperature in the axial and radial directions. As shown in Fig. 12, the maximum bed temperature is inversely proportional to the inlet velocity; it gradually decreases with an increase in inlet velocity. The maximum bed temperature in the bed is 443.62 K at the inlet velocity of 1.5 m/s, which is 10.47 K higher than inlet temperature. The maximum temperature is 440.51 K at the inlet velocity is 2 m/s; it is 3.11 K lower than the maximum temperature of 1.5 m/s. The maximum temperature is 438.68 K at the inlet velocity of 2.5 m/s; it is 1.68 K lower than the maximum temperature of 1.5 m/s. Therefore, as the inlet veloc-

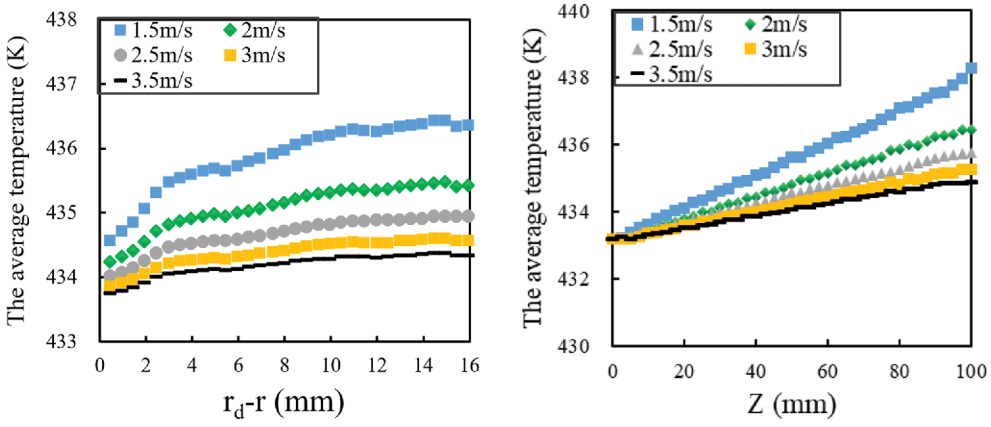

(a) The radial average temperature (b) The axial average temperature

Fig. 11. The average temperature distribution of fluid at different inlet velocity.

Table 5. Molar fraction and VAc selectivity on the outlet at different space velocities

Velocity (m/s)	C_2H_4 (10^{-1})	VAc (10^{-4})	CO_2 (10^{-4})	Selectivity (%)
1.5	7.0441	9.4217	1.7038	91.71
2	7.0478	6.7268	1.1511	92.12
2.5	7.0499	5.2324	0.8674	92.35
3	7.0511	4.2799	0.6945	92.50
3.5	7.0521	3.6182	0.5780	92.60

ity increases, the temperature difference gradually decreases.

Table 5 shows the mole fractions of C_2H_4, VAc and CO_2 at the outlet and the selectivity of vinyl acetate at different inlet velocities. As the velocity increases, the conversion of ethylene in the reactor decreases and the selectivity of vinyl acetate increases from 91.71% to 92.60%. Increasing the inlet velocity results in shorter contact time between the reactants and the catalyst, which in turn reduces the conversion rate and reduces the amount of heat released by the reaction. On the other hand, a higher inlet velocity is beneficial for the removal of heat, resulting in a lower bed temperature and a higher selectivity of vinyl acetate.

7. Effects of Inlet Temperature

The inlet temperature is a dominant parameter in the synthesis of vinyl acetate from ethylene, which directly affects reaction rate, conversion, selectivity and bed temperature. To study the effect of inlet temperature on the reactor performance, the inlet temperature was set to 423.15 K, 428.15 K, 433.15 K, 438.15 K, and 443.15 K. Fig. 13 shows that the axial average temperature gradually increases at different inlet temperatures, and the temperature difference increases with increasing inlet temperature. As can be seen from Fig. 14, with the inlet temperature increasing, the maximum bed temperature also increases gradually.

Table 6 shows the mole fractions of C_2H_4, VAc and CO_2 at the outlet and the selectivity of vinyl acetate at different inlet temperatures. The C_2H_4 conversion rate and the yield of VAc increase with the increase of the inlet temperature, the by-product CO_2 content increases and the selectivity of VAc decreases with the increase of

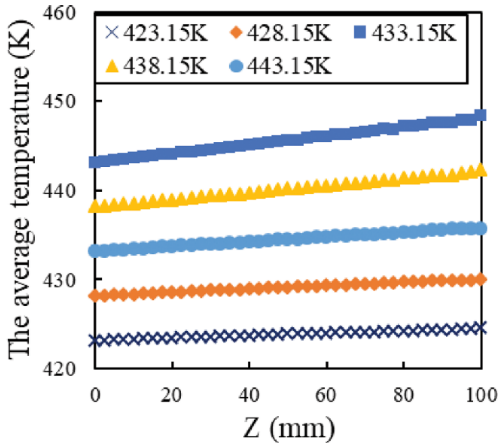

Fig. 13. The axial average temperature distribution at different temperatures.

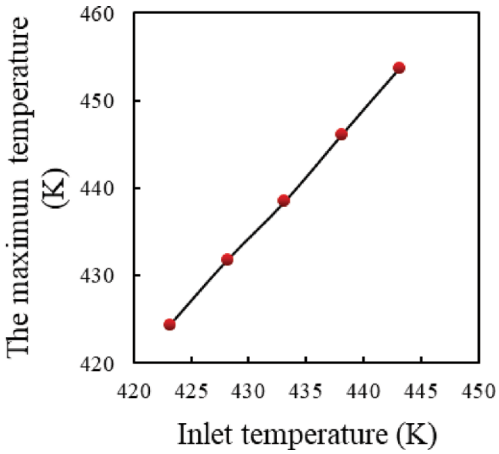

Fig. 14. The maximum temperatures in the fixed-bed at different inlet temperatures.

the inlet temperature. The main reaction apparent activation energy (E_{VAC}=71.94 kJ/mol) is less than the side reaction apparent activation energy (E_{CO2}=109.37 kJ/mol). The reaction rates of the main reaction and side reaction both increase, but the reaction rate of side reaction increases more than the main reaction. Therefore, if the inlet temperature is increased, the selectivity of VAc will decrease. Our finding led us to conclude that lower temperature will reduce the space-time yield and is not conducive to productivity improvement. Therefore, in the production process, because the activity of the catalyst is higher, a lower inlet temperature can be selected in the initial stage of the reaction. As the reaction progresses, the activity of the catalyst gradually decreases; in order to ensure the space-time yield, it is necessary to increase the inlet temperature appropriately.

8. Effects of the Feed Ratio of Ethylene to Oxygen

To keep the ethylene from exploding, the ethylene content in the feed gas must be greatly excessive in the synthesis of vinyl acetate from ethylene. For example, the ratio of ethylene to oxygen is at least 12 : 1 at 0.8 Mpa and 433.15 K. However, the partial pressure of oxygen is a dynamic term which accelerates the reaction rate. Therefore, in this work the effect of the feed ratio of the feed gas was studied. All other parameters remained unchanged; the molar ratio of ethylene, oxygen and acetic acid was set to 12 : 1 : 4, 13 : 1 : 4, 14 : 1 : 4, respectively. And in order to increase the oxygen content in feed gas, nitrogen was added to the feed gas; the molar ratio of ethylene : oxygen:acetic acid : nitrogen was 8 : 1 : 2.5 : 1.

Table 6. Molar fraction and VAc selectivity on the outlet at different inlet temperatures

Reaction temperature (K)	C_2H_4 (10^{-1})	VAc (10^{-4})	CO_2 (10^{-4})	Selectivity (%)
423.15	7.0531	3.0230	0.2485	96.05
428.15	7.0526	3.3353	0.3976	94.37
433.15	7.0499	5.2324	0.8674	92.35
438.15	7.0472	6.9597	1.5254	90.12
443.15	7.0450	8.3305	2.1423	88.61

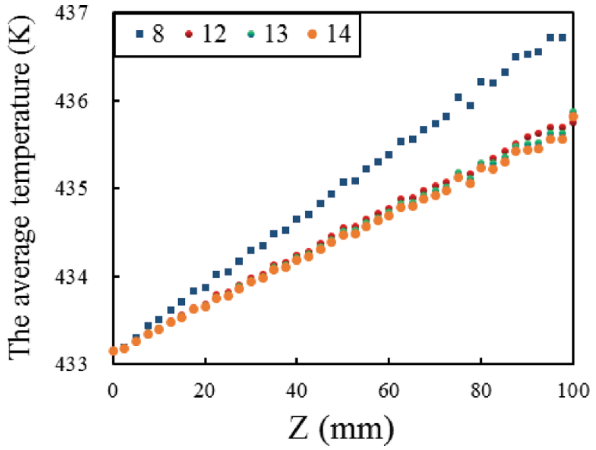

Fig. 15. The axial average temperature distribution in the bed at different feed ratios.

Table 7. Molar fraction and VAc selectivity on the outlet at different feed gas ratios

$C_2H_4 : O_2 : CH_3COOH : N_2$	C_2H_4 (10^{-1})	VAc (10^{-4})	CO_2 (10^{-4})	Selectivity (%)
14 : 1 : 4 : 0	7.3599	4.6561	0.8577	91.57
13 : 1 : 4 : 0	7.2129	4.9276	0.8629	91.95
12 : 1 : 4 : 0	7.0499	5.2324	0.8674	92.35
8 : 1 : 2.5 : 1	6.2872	7.4247	0.9114	94.22

Fig. 15 shows the bed temperature profile at different feed ratios. When the ratio of ethylene to oxygen is between 12 and 14, the bed temperature does not change much with the oxygen content increasing. When the ratio of ethylene to oxygen is raised to 8 : 1, the bed temperature is significantly increases, and the maximum temperature is 441.06 K. From Fig. 15 and the reaction kinetic model, we conclude that when the oxygen content in the feed gas is low, the reaction rate is greatly affected by bed temperature. When the oxygen content in the feed gas is high, the reaction rate begins to be mainly affected by the oxygen concentration.

Table 7 shows the molar fraction of C_2H_4, VAc and CO_2 at the outlet and VAc selectivity at different feed ratios. From Table 7, one can know that when the ratio of ethylene to oxygen is decreased from 12 : 1 to 8 : 1, the conversion of C_2H_4 and the molar fraction of VAc both increase, and the selectivity of vinyl acetate increases from 91.57% to 94.22%. Since the oxygen partial pressure indices are 1 and 0.5 in the main and side reaction kinetic equations, respectively, the main reaction is more sensitive to oxygen concentration than the side reaction. Therefore, to accelerate the reaction rate and increase the conversion of C_2H_4 and the selectivity of VAc, we can add nitrogen to feed gas to reduce the explosion interval of C_2H_4 and increase the partial pressure of O_2.

CONCLUSION

The synthesis of vinyl acetate (VAc) from ethylene was studied by CFD. The results show that in the early stage of the reaction, the catalyst activity is high. To increase the selectivity of VAc, a lower inlet temperature can be selected. As the reaction proceeds, in order to ensure the space-time yield, the inlet temperature can be appropriately increased. Another way to increase selectivity is to increase the catalyst particle diameter or use a composite packed bed. As the inlet velocity increases from 1.5 m/s to 3.5 m/s, the conversion rate of vinyl acetate increases from 91.71% to 92.60% benefit from the removal of heat. Adding an inert gas to the feed gas can increase the oxygen concentration and reduce the explosion interval of C_2H_4. The stable area of the reaction system is enlarged. This method helps to improve the selectivity of vinyl acetate and conversion of C_2H_4.

NOMENCLATURE

∇ : divergence
c_g : specific heat capacity of vapor phase [J·kg^{-1}·K^{-1}]
c_p : specific heat capacity of fluid [J·kg^{-1}·K^{-1}]
c_s : specific heat capacity of solid phase [J·kg^{-1}·K^{-1}]
d_p : particle diameter [m]
d_t : tube diameter [m]
$C_{1\varepsilon}$, $C_{2\varepsilon}$, $C_{3\varepsilon}$: empirical constant
D_i : diffusion coefficient of component *i* [m^2·s^{-1}]
E_{CO2} : the apparent activation energy of side reaction
E_{VAC} : the apparent activation energy of main reaction
F : catalyst surface area [m^2]
G_b : the turbulent kinetic energy generation term caused by buoyancy gives rise
G_k : the turbulent kinetic energy generation term caused by mean velocity gradient
ΔH : standard enthalpy of formation [kJ·mol^{-1}]
h : the height of the bed [m]
h_d : the section increased in the lower stage of the tube
h_g : gas phase mass transfer coefficient [W/m^{-2}·K^{-1}]
h_s : solid phase mass transfer coefficient [W/m^{-2}·K^{-1}]
h_u : the section increased in the upper stage of the tube
M_i : mass fraction of component *i*
N : the tube-to-particle diameter ratio
$\overline{p}$: the average void ratio
r_1 : reaction rate of main reaction [mol·g^{-1}min^{-1}]
r_2 : reaction rate of side reaction [mol·g^{-1}min^{-1}]
Re_p : particle Reynolds number
$S\kappa$: turbulent kinetic energy source items [J]
$S\varepsilon$: turbulent dissipation rate source term
T : temperature [°C]
T_c : the temperature of the volume near the wall [K]
T_g : the temperature of vapor phase [K]
$\overline{u}_i$: mean velocity component of *i* direction [m·s^{-1}]
u_i' : fluctuation velocity of *i* direction [m·s^{-1}]
VAc : vinyl acetate
w_i : molar mass of component [kg·mol^{-1}]
y_c : the normal distance of the volume near the wall [m]
Y_M : contribution of pulsating expansion in compressible turbulence

Greek Letters

κ : turbulence kinetic energy [J]

ε : turbulent dissipation rate
ρ : density [kg·m^{-3}]
v : velocity [m·s^{-1}]
v_{in} : inlet velocity [m·s^{-1}]
μ : dynamic viscosity [Pa·s]
$\sigma\varepsilon$: Prandtl number corresponding to the turbulent dissipation rate
$\sigma\kappa$: Prandtl number corresponding to turbulent kinetic energy

REFERENCES

1. N. Panda and S. A. Yadav, *Asian J. Chem.*, **8**, 296 (2019).
2. H. F. Rase and M. Hayes, *Platin Met. Rev.*, **45**, 83 (2001).
3. S. Geng, M. U. Haque and K. Oksman, *Compos. Sci. Technol.*, **126**, 35 (2016).
4. T. V. Panova, A. A. Efimova and A. V. Efimov, *Colloid Polym. Sci.*, **7**, 1 (2019).
5. A. R. G. Caranton, J. Dille, J. Barreto, F. Stavale, J. C. Pinto and M. Schmal, *ChemCatChem*, **10**, 5256 (2018).
6. Y. F. Han, J. H. Wang, D. Kumar, Z. Yan and D. W. Goodman, *J. Catal.*, **232**, 467 (2005).
7. Y. F. Han, D. Kumar, C. Sivadinarayana and D. W. Goodman, *J. Catal.*, **224**, 60 (2004).
8. X. Dong, Y. Wang, Y. Yu and M. H. Zhang, *Ind. Eng. Chem. Res.*, **57**, 7363 (2018).
9. K. Motahari, H. Atashi, F. Fazlollahi and M. Sarkari, *Jind Eng. Chem.*, **18**, 266 (2012).
10. K. Motahari, G. Rempel, S. Lashkarara, K. Ghaseminezhad, A. Borumandnejad and B. Hatami, *Can. J. Chem. Eng.*, **94**, 506 (2016).
11. D. Stacchiola, F. Calaza, M. Neurock and W. T. Tysoe, *J. Am. Chem. Soc.*, **132**, 2202 (2010).
12. S. Nakamura and T. Yasui, *J. Catal.*, **54**, 605 (1982).
13. Q. L. Pham, Y. Haldorai and V. H. Nguyen, *Korean J. Chem. Eng.*, **31**, 2101 (2014).
14. A. Talebian, A. R. Keshtkar and M. A. Mohammad, *Korean J. Chem. Eng.*, **33**, 2205 (2016).
15. S. A. Jafari and A. Jamali, *Korean J. Chem. Eng.*, **33**, 1296 (2016).
16. A. G. Dixon, M. Nijemeisland and E. H. Stitt, *Adv. Chem. Eng.*, **31**, 307 (2006).
17. S. A. Logtenberg and A. G. Dixon, *Chem. Eng. Process.*, **37**, 7 (1998).
18. P. X. Jiang, R. N. Xu and W. I. Gong, *Chem. Eng. Sci.*, **61**, 7213 (2006).
19. A.Guardo, M. Coussirat, M. A. Larrayoz, F. Recasens and E. Egusquiza, *Chem. Eng. Sci.*, **60**, 1733 (2005).
20. P. R. Gunjal, V. V. Ranade and R. V. Chaudhari, *AIChE J.*, **51**, 365 (2005).
21. H. Atashi, M. Sarkari, K. Motahari, F. F. Tabrizi and F. Fazlollahi, *J. Korean Chem. Soc.*, **55**, 92 (2011).
22. K. Motahari, G. Rempel, S. Lashkarara, K. Ghaseminezhad, A. Borumandnejad and B. Hatami, *Can. J. Chem. Eng.*, **94**, 506 (2016).
23. Y. F. Han, D. Kumar and D. W. Goodman, *J. Catal.*, **230**, 353 (2005).
24. B. Partopour, *AIChE J.*, **63**, 87 (2017).
25. B. Partopour and A. G. Dixon, *Ind. Eng. Chem. Res.*, **55**, 7296 (2016).
26. D. Ying, F. J. Keil, O. Korup, F. Rosowski and R. Horn, *Chem. Eng. Sci.*, **142**, 299 (2016).
27. R. Y. Hong, W. Yang, Y. Q. Zhuang and H. Z. Li, *Comput. A. Chem.*, **23**, 481 (2006).
28. P. Behnam and A. G. Dixon, *AIChE J.*, **63**, 87 (2017).
29. G. D. Wehinger, M. Kraume, V. Berg, O. Korup, K. Mette, R. Schlogl, M. Behrens and R. Horn, *AIChE J.*, **62**, 4436 (2016).
30. G. D. Wehinger, T. Eppinger and M. Kraume, *Chem. Eng. Sci.*, **122**, 197 (2015).
31. K. Vollmari, T. Oschmann, S. Wirtz and H. K. Emden, *Powder Technol.*, **271**, 109 (2015).
32. X. M. Zhou, Y. J. Duan, X. L. Huai and X. F. Li, *Particuology*, **11**, 715 (2012).
33. V. Mandar, S. T. Johansen and S. Amini, *Ind. Eng. Chem. Res.*, **52**, 12041 (2013).
34. A. G. Dixon, *Can. J. Chem. Eng.*, **66**, 705 (1988).
35. G. D. Wehinger, T. Eppinger and M. Kraume, *Chem. Eng. Sci.*, **122**, 197 (2015).
36. A. G. Dixon, M. Nijemeisland and E. H. Stitt, *Comput. Chem. Eng.*, **48**, 135 (2013).
37. S. H. Cheng, H. Chang and Y. H. Chen, *Computational fluid dynamics-based multiobjective optimization for catalyst design*, 21st International Symposium on Chemical Reaction Engineering, Philadelphia, PA, 13-16 July (2010).
38. Z. X. Zhao, Q. L. Dai, S. D. Wang, B. Y. Lin and G. T. Chen, *Chem. React. Eng. Technol.*, **2**, 128 (1995).